NASA Technical Memorandum 4407

Total Temperature Probes for High-Temperature Hypersonic Boundary-Layer Measurements

Cindy W. Albertson and Willard A. Bauserman, Jr.
Langley Research Center
Hampton, Virginia

Summary

This paper presents design details and test results of two types of total temperature probes that were used for hypersonic boundary-layer measurements in the Langley 8-Foot High-Temperature Tunnel. The intent of each probe design was to minimize the total error and maintain a minimal size for measurements in boundary layers 1.0 in. thick and less. A single platinum 20-percent-rhodium shield, used in both designs, minimized radiation heat transfer losses during exposure to the high-temperature test stream. The main design difference was the vent-to-inlet area ratio. To reduce vertical averaging effects on the data, the shield of the initial design (probe A) was flattened at the flow entrance to an interior height of 0.03 in., which resulted in a vent-to-inlet area ratio of 50 percent; to reduce vertical averaging effects near the wall even further, the shield of the later design (probe B) was flattened to 0.02 in., which resulted in an area ratio of 60 percent. A stainless steel structural support sleeve that was installed on probe A was excluded from probe B, which resulted in a probe B outer diameter of 0.059 in., to allow closer placement of the probes to each other and to the wall. These small design changes to improve the resolution did not affect probe performance. Tests were conducted at boundary-layer-edge Mach numbers of 5.0 and 6.2. The nominal free-stream total temperatures were 2600° and 3200°R. The local Reynolds number $N_{Re,x}$, based on boundary-layer-edge conditions and distance from the leading edge, ranged from 3.5×10^6 to 28.6×10^6. The reliability of the probes was extremely good. After 11 runs, no type A probes and only 1 of 10 type B probes failed. Temperature measurements in fully turbulent boundary layers compared well with Crocco-Busemann predictions. The best performance in terms of recovery factor occurred when the wire-based Nusselt number $N_{Nu,w}$ was at least 0.04. Suggestions for future probe designs are included in "Recommendations."

Introduction

Total temperature measurements are required for many compressible flow experiments, including those in relatively thin boundary layers. Many total temperature probes that are designed for boundary-layer measurements are unshielded to reduce size and to minimize spatial averaging, time constant, and disturbances to the boundary layer. (See refs. 1 through 4.) Unshielded probes incur radiation errors that can be corrected in the data reduction process; however, the errors become larger and more difficult to correct with increasing temperature. To minimize the radiation error, single-shielded probes are often used. (See refs. 5 through 10.) Winkler (ref. 5) designed one of the earliest shielded probes which was vented to allow the high-temperature gas to flow continuously through the probe. Replenishing the high-temperature gas within the probe minimized errors. Winkler's probe shield was constructed from silica to minimize conduction and was coated with platinum to minimize radiation. Later designs incorporated additional features to improve accuracy. East and Perry (ref. 6) designed a probe with a heating element that was wrapped around the radiation shield to minimize radiation losses from the thermocouple junction. Weinstein (ref. 8) mounted a thermocouple at the base of the probe to aid in computing corrections for conduction losses. Many of these probes are too large to resolve distributions in thin boundary layers. Resolution of the boundary layer is particularly difficult with probe installation in a fixed rake; however, fixed rakes are often necessary when high wall temperatures and the associated thermal expansion problems complicate the design of a traversing rake.

The total temperature probes described herein were developed for hypersonic boundary-layer measurements on a flat plate (ref. 11) in the Langley 8-Foot High-Temperature Tunnel (8'HTT). The probe design concerns were the high total temperature of the test stream, the response time, the vibration attributed to flow unsteadiness, and the small size required to define the total temperature in boundary layers 1.0 in. thick and less. Two probe designs were constructed with a vented, single shield to minimize radiation heat transfer losses and maintain a reasonably small size. To minimize vertical averaging effects, both probe shields were flattened at the flow entrance. The smaller probe had a maximum outside body diameter of 0.059 in. and an interior sampling height of 0.02 in.; these probes are smaller than other shielded probes that are found in the literature. Platinum 13-percent-rhodium versus platinum (type R) thermocouple wire was required in both probe types for high total temperature measurement. A wire diameter of 0.010 in. was chosen to withstand flow-induced vibration.

The probes were mounted in fixed rakes that were installed at various locations on the flat-plate model. The tests were conducted at a nominal free-stream Mach number of 7, and the model was pitched at nominal angles of attack of 5° and 13°. The corresponding boundary-layer-edge Mach numbers were 6.2 and 5.0, respectively. Near the wall, the Mach number ahead of the probes was as low as 1.7. The local Reynolds number $N_{Re,x}$, based on both the

conditions at the boundary-layer edge and the distance from the leading edge, ranged from 3.5×10^6 to 28.6×10^6. The local Reynolds number $N_{Re,p}$, based on thermocouple junction diameter and estimated probe internal flow conditions, ranged from 63 to 2470.

Symbols

A	area, in^2
C	circumference, in.
c	specific heat, Btu/lbm-°R
c_p	specific heat at constant pressure, Btu/lbm-°R
D_1 through D_5	constants used in eqs. (A5) and (A11)
diam	diameter, in.
d_J	junction diameter, in.
d_w	wire diameter, in.
E	measurement error, °R
F	configuration factor
H	enthalpy, Btu/lbm
$\overline{H}$	distance from tunnel centerline, in.
h	heat transfer coefficient, Btu/sec-ft^2-°R
I	cross-sectional moment of inertia, in^4
i.d.	inner diameter
k	thermal conductivity, Btu/sec-ft-°R
L	cantilevered length, in.
L_1, L_2	thermocouple wire lengths, in. (see fig. 13(a))
M	Mach number
M_2	Mach number behind normal shock (see fig. 9)
m	bending moment, in-lbf
N	velocity power law exponent, equation (C2)
N_{Bi}	Biot number, $(h_p d_w/4 k_w)^{1/2}$

$N_{Nu,p}$	Nusselt number based on thermocouple junction diameter and local flow conditions inside probe, upstream of junction, $h_p d_J/k_p$
$N_{Nu,w}$	Nusselt number based on thermocouple junction diameter, thermocouple wire conductivity, and local flow conditions inside probe, upstream of junction, $h_p d_J/k_w$
N_{Pr}	Prandtl number, $\mu c_p/k$
$N_{Pr,p}$	Prandtl number based on local flow conditions inside probe, $(\mu c_p/k)_p$
$N_{Re,p}$	Reynolds number based on thermocouple junction diameter and local flow conditions inside probe, upstream of junction, $\rho_p U_p d_J/\mu_p$
$N_{Re,x}$	local Reynolds number based on distance from leading edge and evaluated at boundary-layer-edge temperature, $\rho_e U_e x/\mu_e$
$N_{Re,\infty}$	free-stream unit Reynolds number, $\rho_\infty U_\infty/\mu_\infty$, 1 per foot
n	distance along thermocouple wires, in. (see fig. 13(a))
o.d.	outer diameter
p	pressure, psia
$\dot{q}$	heat transfer rate, Btu/sec-ft^2
r	radius, in.
T	temperature, °R
T_2	static temperature behind normal shock, °R (see fig. 9)
t	time, sec
U	velocity, ft/sec
V	volume, in^3
w	distributed load per unit length, lbf/in.

x, y	plate surface coordinates, ft (see fig. 4)	tk	known total condition
Y	modulus of elasticity, psi	t_∞	total free-stream condition
y_{max}	maximum deflection, in. (eq. (D3))	t_2	total condition behind normal shock
z	distance measured normal from plate surface, in. (see fig. 4)	U	velocity
		w	thermocouple wire
α	angle of attack, deg	∞	free stream
δ_T	thermal boundary-layer thickness, in.		
δ_U	velocity boundary-layer thickness, in.		
ε	emittance		
μ	viscosity, lbm/sec-ft		
ρ	density, lbm/ft^3		
σ_B	Stefan-Boltzmann constant, Btu/sec-ft^2-°R^4		
σ_{max}	maximum bending stress, psi (eq. (D1))		
τ	thermal response time, sec		

Subscripts:

aw	adiabatic wall
c	convection
e	boundary-layer edge, just outside boundary layer
J	thermocouple probe junction
k	conduction
l	local condition
p	flow condition inside probe, just upstream of thermocouple junction
r	radiation
si	condition at interior of radiation shield
so	condition at exterior of radiation shield
t	total condition
tc	total condition in combustor
te	total condition at boundary-layer edge

Description of Experiment

Total Temperature Probes and Rakes

Design Considerations

The goal of the total temperature probe is to produce a flow environment at the thermocouple junction which will enable the thermocouple to measure the total temperature accurately. The accuracy of the probe depends on the balance of the convective heat transfer between the gas and the junction, the radiation from the junction to the shield, and the conduction from the junction along the thermocouple wires to the cooler probe support. The difference between the total temperature of the gas T_t and the junction temperature T_J is referred to as the total error E_t. The equation for the total error is given as

$$E_t = E_U + E_k + E_r \qquad (1)$$

In equation (1), E_U, E_k, and E_r represent the decoupled errors due to the velocity of the flow inside the probe, conduction along the thermocouple wires, and radiation to the junction surroundings, respectively. A discussion of these errors and how to reduce them is given below.

Error due to flow velocity. The error due to flow velocity E_U is the difference between the total temperature of the gas to be measured T_t and the adiabatic wall temperature of the thermocouple wires T_{aw}. For all Prandtl numbers, T_{aw} approaches T_t with decreasing velocity. Therefore, E_U can be decreased by reducing the flow velocity inside the probe. However, the convective heat transfer to the thermocouple bead is also reduced when the flow velocity decreases, which leads to an increase in the conduction and radiation errors. Therefore, the velocity must not be reduced to the extent that the total error increases for the design conditions. Because this velocity cannot be measured easily, experiments to reduce E_U emphasize the probe vent-to-inlet area ratio. (See refs. 5 and 10.) These

experiments indicate that the optimum area ratio varies with probe size.

Conduction error. The conduction error is a function of the length and diameter of the thermocouple wires, the thermophysical properties of the wires, convective heat transfer to the wires, and the probe support temperature. (See eq. (A11).) The most practical way to reduce the conduction error is to maximize the length and minimize the diameter of the wires, because selection of the thermophysical properties of the wire is limited. The selection of thermocouple wire type is usually determined by the temperature of the gas to be measured.

Radiation error. The radiation error is a function of the emittance of both the shield and the thermocouple wires, the radiation view factor between the shield and the wires, and the temperature of the radiation shield. Selection of a shield material with a low emittance to reduce heat loss to the probe surroundings can reduce this error. However, the strength of the shield material at high temperatures must also be considered, particularly in an environment with large flow-induced vibrations. The junction and wires should be enclosed as much as possible within the shield. However, the shield length and diameter must be selected such that the junction is not immersed in the shield boundary layer. The radiation error can be reduced further by increasing the temperature of the radiation shield, particularly near the thermocouple junction and wires. The temperature of the shield can be increased by increasing the internal flow velocity, which increases the heat transfer to the shield, and by decreasing the heat conducted along the shield to the cooler support. The heat conducted along the shield can be reduced by increasing the shield length and reducing the shield thickness. An increase in the number of concentric shields increases the temperature of the inner shield and reduces the radiation error; however, the diameter of the probe is increased, which is undesirable for detailed boundary-layer measurements.

Probe and Rake Description

The present probe design is a compromise between a reduction of errors, size minimization, and the ability to withstand flow-induced vibrations. For the chosen design, the total calculated error ranges from 0.4 to 6.2 percent. Conduction losses that occur at the low probe Reynolds number conditions, particularly deep within the boundary layer at a relatively low total temperature, cause most of the total error. Details of these errors are given in appendix A, and methods to reduce errors in future designs are described in "Recommendations."

Two probe types were used to measure the total temperature distributions through the boundary layer. These probes are illustrated in figure 1 and are shown schematically in figure 2. Both probes contained a platinum–13-percent rhodium versus platinum thermocouple (type R) that was mounted inside a single 0.005-in-thick radiation shield. A thermocouple wire diameter of 0.010 in. was chosen to withstand the flow-induced vibration. Platinum–20-percent rhodium was selected as the shield material because of its relatively low emittance and relatively high strength at high temperatures. The main difference between the two probes was the vent-to-inlet area ratio. To minimize vertical averaging effects on the data, the shield of the initial probe (probe A) was flattened at the flow entrance to an interior height of 0.03 in. To further reduce vertical averaging effects near the wall, the shield of the later design (probe B) was flattened to 0.02 in. at the flow entrance. Two vent holes with diameters of 0.022 in. were drilled in both probe shields to allow the probes to vent. The resulting vent-to-inlet area ratios were 50 and 60 percent. Area ratios in this range were shown by Bartlett, Edwards, and Hillier (ref. 10) to provide optimal temperature recovery, although Bartlett's probes had interior heights at the flow entrance of 0.035 in., which is larger than the probes described herein. Another difference was that probe A incorporated a 308 stainless steel structural support sleeve to withstand the flow-induced vibrations and to provide a bearing surface to tighten the set screw that holds the probe in the rake. The outside body diameter of probe A with this sleeve was 0.094 in. (See fig. 2(a).) The sleeve was excluded from probe B to allow closer placement of the probes to each other and to the wall of the plate. (See fig. 2(b).) The outside body diameter of probe B was 0.059 in.

To assemble the probes, the thermocouple wires were threaded through the two-holed ceramic insulation and were then joined to form the thermocouple junction. For probe A, the stainless steel structural support sleeve was then installed and bonded to the fiberglass-covered thermocouple wire with epoxy. (See fig. 2(a).) The platinum radiation shield was then installed and spot welded to the support sleeve. Because probe B lacked a support sleeve, the assembly process was simpler. For this probe, the platinum shield was bonded to the ceramic insulation and fiberglass-covered thermocouple wire with epoxy. (See fig. 2(b).)

The probes were mounted in two different fixed-rake struts, rake A and rake B. (See figs. 3(a) and 3(b).) Rake A, the initial design, contained

11 type A probes. Rake B contained 15 temperature probes; 8 of the 15 were type B probes within 0.54 in. of the wall. The remaining probes in rake B were type A with the exception of one type B probe outside the boundary layer at $z = 2.200$ in. The probe types and their locations in each rake are given in table I. Both rakes were machined to facilitate replacement of damaged temperature probes. Cast bronze alloy 5 was selected as the rake material because of its heat-sink characteristics, which enable the rake to survive during the relatively short exposure times to the high-temperature flow.

Test Configuration

The test model was a large, heavily instrumented flat plate that was installed on the panel holder, a generalized test apparatus for the 8'HTT. (See fig. 4.) A sharp leading edge was attached to the front of the panel holder. The model was 9.7 ft long and 4.3 ft wide. Boundary-layer rake assemblies, which consisted of total pressure, static pressure, and total temperature probes, were used to survey the boundary layer at various locations on the plate. (See figs. 4 and 5.) Model details and additional instrumentation are presented in reference 11.

Data Acquisition and Reduction

All data channels, including thermocouple outputs, were sampled and recorded 20 times per second per channel with a 12-bit digital data acquisition system. All signals were filtered with 10-Hz low-pass filters and digitized before being recorded on magnetic tape. The total estimated accuracy of the data acquisition equipment is within 1 percent. Additional details of this equipment and its accuracy are given by Nowak. (See ref. 12.)

Thermocouple outputs from the total temperature probes were converted to temperatures from the thermocouple tables given in reference 13 for a type R thermocouple. Pretest calibrations of the thermocouple wire used in the probes were conducted up to 2300°R. These calibrations indicated small, consistent variations from the tables. Additional details regarding the data reduction are given in reference 11.

Test Facility

The tests were conducted in the 8'HTT, which is shown schematically in figure 6. This facility is a large blowdown wind tunnel that provides true-temperature flight simulation at a nominal free-stream Mach number of 7 and at pressure altitudes

from 80 000 to 126 000 ft. The high-energy test medium consists of a mixture of methane and air burned under high pressure in the combustor. The test medium then expands through an axisymmetric, conical contoured nozzle to achieve the test chamber Mach number. The flow in the test chamber is a free jet that enters a straight-tube supersonic diffuser, where it is pumped to the atmosphere by a single-stage annular air ejector. The tunnel can be operated at total temperatures from 2400° to 3600°R and at free-stream dynamic pressures from 240 to 1800 psf. The corresponding free-stream Reynolds number $N_{Re,\infty}$, based on a model length of 10 ft, ranges from 3×10^6 to 30×10^6.

Models are positioned below the test chamber (fig. 7) during tunnel startup and shutdown to minimize aerodynamic loads. When flow conditions are established, the model is inserted into the flow by a hydraulically actuated elevator. Before tunnel shutdown, the model is withdrawn from the flow. The maximum test time for the facility is 120 sec. The present model was positioned 1.0 ft from the nozzle exit (fig. 7) and was exposed to the flow for no more than 10 sec. Additional details of the 8'HTT can be found in reference 14.

Test Conditions

The tests were conducted at nominal total temperatures of 2600° and 3200°R. The nominal free-stream Mach number was 7, and the free-stream Reynolds number $N_{Re,\infty}$, based on plate length, ranged from 5.5×10^6 to 18.0×10^6. To obtain relatively high local Reynolds numbers, the model was pitched at angles of attack of 5° and 13°, which produced boundary-layer-edge Mach numbers of approximately 5.0 and 6.2, respectively. Most tests were conducted at an angle of attack of 13°. This angle of attack produced local Reynolds numbers high enough for large areas of equilibrium turbulent boundary-layer flows over the plate, as discussed in reference 11. The local Reynolds number $N_{Re,x}$, based on boundary-layer-edge conditions and distance from the leading edge, ranged from 3.5×10^6 to 28.6×10^6; the local Reynolds number $N_{Re,p}$, based on internal probe diameter and flow conditions, ranged from 63 to 2470. The local flow conditions and those upstream in the combustor are given in table II. Details of how these conditions were determined and their accuracy are given in reference 11.

Results and Discussion

Selected sets of data obtained from the total temperature probes are discussed in the following

5

sections to aid in the assessment of probe performance. The measurements shown herein were obtained along the plate centerline at $y = 0$ in. (The coordinate system is defined in fig. 4.) A complete data tabulation for each run is given in appendix H of reference 11.

The probe reliability was extremely good. After 11 runs, no type A probes failed and only 1 of 10 type B probes failed.

Temperature Histories

A typical temperature history T_J from a type A total temperature probe, placed outside the boundary layer at $z = 2.500$ in. and 72 in. from the nozzle exit plane, is shown in figure 8(a). The data are shown for an intermediate Reynolds number $N_{Re,p}$ of 1016; $N_{Re,p}$ corresponds to the thermocouple junction diameter and conditions inside the probe that were determined from total temperature measurements, total pressure measurements, and the vent-to-inlet area ratio. The total temperature measured upstream in the combustor T_{tc} is also shown in figure 8(a). In figure 8(b), the approximate distance of the probe from the test section centerline $\overline{H}$ is shown. (The oscillations shown in the probe position near $\overline{H} = 0$ in. are probably caused by a problem that results from the potentiometer used as a model position indicator. No evidence exists to indicate that the test panel deflected this amount during a run.) Before the model entered the test stream, the temperature indicated by the probe was approximately 500°R (fig. 8(a)). The probe began to respond to the temperature of the test core approximately 0.65 sec from initial model movement, or approximately 0.2 sec before the probe crossed the nozzle edge. This response indicates that the jet boundary expanded beyond the nozzle edge. After about 2.1 sec, or approximately 1.45 sec after the probe first began to react to the flow, the probe temperature nearly matched that of T_{tc}.

The thermal response times of the probes could not be accurately determined from the present experiment because of numerous complications. The main complication was that the probes were not exposed to a step change in temperature. Total temperature surveys of the test core (ref. 11) indicate that the free-stream total temperature $T_{t,\infty}$ (fig. 6) is lower than T_{tc} near the edge of the nozzle and gradually increases to approximately the level of T_{tc} near the test section centerline. Also, the exact temperature profile to which the probes are exposed during entry into the test stream is not precisely known, because free-stream total temperature surveys are taken while the

model is below the test core. However, if a step input in temperature is assumed, the thermal response time τ, corresponding to the time required for the junction to reach 63.2 percent of the surrounding gas temperature, is estimated between 0.3 and 1.5 sec for the two extremes in flow conditions. (See appendix B.) Likewise, the predicted value for 5τ, which corresponds to the time required for the junction temperature to reach 99.3 percent of the gas temperature, should range from 1.5 to 7.5 sec, which is within the desired model exposure time.

Correlation of Temperature Recovery Factor

The difference between the junction temperature and the true stagnation temperature is a function of the convective heat transfer to the junction and the losses due to the conduction, radiation, and velocity. (See Winkler, ref. 5.) As convection increases, the relative losses decrease, which results in a higher temperature recovery. Winkler assumed that the losses are mostly caused by conduction and showed that the recovery factor $T_J - T_{\infty,l}/T_{tk} - T_{\infty,l}$ is proportional to the Nusselt number $N_{Nu,w}$ at the probe junction that is based on wire conductivity, where $N_{Nu,w} = h_p d_J/k_w$. Here, T_J is the total temperature indicated by the probe thermocouple junction, T_{tk} is a known total temperature, and $T_{\infty,l}$ is the local static temperature just upstream of the probe. (See fig. 9.) Also, h_p is the convective heat transfer to the junction, d_J is the junction diameter, and k_w is the conductivity of the thermocouple wire. Winkler then showed that the recovery factor correlates to a simpler parameter that is based on wire Nusselt number, given as $\rho_J \times T_J^{-1.75}$, where ρ_J is the density of the gas at the junction. A simpler parameter, $p_{t_2} \times T_J^{-1.75}$, can be derived from the equation of state. Here, p_{t_2} is the total pressure behind a normal shock and the assumed pressure of the gas ahead of the junction.

To assess the performance of the total temperature probes, the recovery factor $T_J - T_{\infty,l}/T_{tk} - T_{\infty,l}$ is plotted as a function of wire-based Nusselt number at the probe junction $N_{Nu,w}$ in figure 10 and as a function of the modified Winkler parameter $p_{t_2} \times T_J^{-1.75}$ in figure 11. The wire-based Nusselt number was determined from equation (A1) in appendix A, which relates $N_{Nu,p}$ to the probe Reynolds number $N_{Re,p}$. Here, $N_{Nu,p}$ is based on the conductivity of the gas within the probe k_p and differs from $N_{Nu,w}$ by a factor of k_p/k_w. The probe Reynolds number was calculated from the measured total temperature, the total pressure measured by a nearby total pressure probe, and the probe internal Mach

number M_2 (fig. 9). The probe internal Mach number was calculated, assuming inviscid flow, from the probe inlet-to-vent area ratio. The data were taken from measurements outside the boundary layer along the plate centerline. The combustor total temperature T_{tc} was used as the known total temperature to compute the recovery factor. The data show scatter in both plots; however, there is no discernible difference in the performance of probes A and B at the high- and low-temperature conditions. As expected, the recovery factors increase with $N_{Nu,w}$ and $p_{t_2} \times T_J^{-1.75}$. The recovery factors range from 0.89 to 1.02 compared with the uncorrected combustor total temperature. Although some of these values were higher than 1.0, most of the factors compare reasonably well with the results from reference 15. The best performance occurs when $N_{Nu,w} \geq 0.04$. The modified Winkler parameter, a more easily calculated variable, should be at least 25×10^{-6} psia-$°R^{-1.75}$ for best performance, at least for the nominal free-stream local Mach numbers of 5.0 and 6.3. Because the correlations are based on conditions inside the probe, these results are expected to apply to other free-stream local Mach numbers.

Distributions of Boundary-Layer Total Temperature

To evaluate the total temperature distributions measured in the boundary layer, the linear Crocco-Busemann enthalpy-velocity relationship (ref. 16) was applied. Additional assumptions and details of this relationship are given in appendix C.

The total temperature data and Crocco-Busemann predictions are shown for Reynolds numbers $N_{Re,x}$ of 28.6×10^6, 13.6×10^6, and 4.5×10^6 in figures 12(a), 12(b), and 12(c), respectively. The boundary-layer thickness δ_U is shown on the plots for reference purposes. The rake B data and predictions show good agreement for the two high Reynolds number cases (figs. 12(a) and 12(b)) in which the thermal and velocity boundary layers were fully developed. (See ref. 11.) The data obtained at the low Reynolds number condition (fig. 12(c)) were transitional (ref. 11). The lack of agreement between the data and prediction at the low Reynolds number condition may result from diminished probe accuracy at such conditions or from a breakdown in the Crocco-Busemann prediction. The Crocco-Busemann prediction is not applicable to transitional boundary layers when the thermal and velocity boundary layers (ref. 17) are nonsimilar. The irregularity in the total temperature profile at $z = 0.8$ in. for the low Reynolds number condition (fig. 12(c)) is also present in the Mach number distribution obtained at

this condition (ref. 11). These irregularities indicate that a weak shock is present in the flow outside the boundary layer.

Recommendations

For future probe designs, both the radiation and conduction errors discussed in appendix A can be reduced by increasing the length of the shield and thermocouple wires, particularly the portion exposed to the flow inside the probe. This increase in length will increase the area available for convection and will reduce the heat conducted down the wires and the shield to the relatively cool rake. This change will also reduce radiation losses from the junction, because the temperature of the radiation shield will be higher. The structural analysis given in appendix D indicates that the length of the shield and wires can be increased to some extent without significantly weakening the probe. However, the material properties used in the analysis are uncertain at 3300°R because they must be extrapolated from lower temperature data. The thermal response time of the junction can be reduced in future probes by forming the junction with a spot weld rather than with a conventional bead weld to reduce the junction size.

The vent-to-inlet area ratio has not been optimized for the probe designs described in this paper. Although the area ratios were within the values recommended in reference 10, the present probes are smaller than those in reference 10, and the flow inside the probe is dominated more by viscosity. Therefore, experiments should be conducted to determine if a larger vent-to-inlet area ratio is required for optimal probe performance.

Concluding Remarks

This paper presents the design details and test results of two types of total temperature probes that were used for hypersonic boundary-layer measurements in the Langley 8-Foot High-Temperature Tunnel. The intent of each probe design was to minimize the total error and maintain a minimal size for measurements in boundary layers 1.0 in. thick and less. A single platinum-20-percent-rhodium shield, used in both designs, minimized radiation heat transfer losses during exposure to the high-temperature test stream. The main design difference was the vent-to-inlet area ratio. To reduce vertical averaging effects on the data, the shield of the initial design (probe A) was flattened at the flow entrance to an interior height of 0.03 in., which resulted in a vent-to-inlet area ratio of 50 percent; to reduce vertical averaging effects near the wall even further, the shield of the later design (probe B) was flattened to 0.02 in.,

which resulted in an area ratio of 60 percent. A stainless steel structural support sleeve that was installed in probe A was excluded from probe B, which resulted in a probe B outer diameter of 0.059 in., to allow closer placement of the probes to each other and to the wall. These small design changes to improve the resolution did not affect probe performance.

Tests were conducted at boundary-layer-edge Mach numbers of 5.0 and 6.2. The nominal freestream total temperatures were 2600° and 3200°R. The local Reynolds number $N_{Re,x}$, based on boundary-layer-edge conditions and distance from the leading edge, ranged from 3.5×10^6 to 28.6×10^6. The local Reynolds number inside the probe $N_{Re,p}$ ranged from 63 to 2470. The reliability of the probes was extremely good. After 11 runs, no type A probes and only 1 of 10 type B probes failed. Predictions of probe thermal response times ranged from 0.3 to 1.5 sec. Temperature recovery factors ranged from 0.89 to 1.02 compared with the uncorrected upstream combustor temperature measurement. The best performance in terms of recovery factor occurred when the wire-based Nusselt number $N_{Nu,w}$ was at least 0.04. The modified Winkler parameter, a more easily calculated variable, should be at least 25×10^{-6} psia-°R$^{-1.75}$ for optimum performance. Temperature measurements in fully turbulent boundary layers compared well with Crocco-Busemann predictions.

The total calculated error of the probes in the test range varies from 0.4 to 6.2 percent. Most of the errors that occur at the low probe Reynolds number conditions are estimated to be caused by conduction losses, particularly deep within the boundary layer where the total temperature is relatively low.

NASA Langley Research Center
Hampton, VA 23681-0001
January 4, 1993

Appendix A

Calculations of Theoretical Probe Errors

To calculate the theoretical measurement errors of the total temperature probes, an error analysis was performed for the two extremes in flow conditions that produced the highest and lowest convective heat loads to the thermocouple junction. The first extreme (case 1) corresponded to a probe outside the boundary layer at the highest probe Reynolds number and at a relatively high total temperature test condition; the second extreme (case 2) corresponded to a probe close to the wall at the lowest probe Reynolds number and at a relatively low total temperature test condition. The probe internal Reynolds numbers $N_{Re,p}$, based on junction diameter, were 2470 and 63 for cases 1 and 2, respectively. The total temperatures used in the theoretical calculations were 3140° and 2340°R for cases 1 and 2, respectively. These temperatures were obtained from the upstream combustor temperature measurement. Because case 2 corresponds to a probe within the boundary layer, the total temperature of 2340°R used in the calculations was derived from the combustor temperature measurement based on the Crocco-Busemann relationship given in appendix C.

Before calculating the errors, $N_{Re,p}$ was calculated to determine the convective heat load to the thermocouple wires. The value of $N_{Re,p}$ was calculated with the measured total temperature T_J, the total pressure behind a normal shock (measured from a nearby total pressure probe) p_{t_2}, the probe internal Mach number, and the fluid and transport properties of methane-air combustion products given in reference 18. (See fig. 9.) For simplicity, p_{t_2} was assumed to be the pressure of the gas ahead of the thermocouple junction. The probe internal Mach number was calculated, assuming inviscid flow, from the probe inlet-to-vent area ratio. The probe Nusselt number $N_{Nu,p}$ was then calculated from the correlation given in reference 15 for wires parallel to the flow as follows:

$$N_{Nu,p} = 0.095 N_{Pr,p}^{0.31} N_{Re,p}^{0.674} \qquad (A1)$$

From equation (A1), the heat transfer coefficient h_p was then calculated.

Finally, the total probe error E_t was assumed to be equal to the sum of the individual decoupled errors as follows:

$$E_t = E_U + E_k + E_r \qquad (A2)$$

In equation (A2), E_U, E_k, and E_r represent the errors from the internal velocity of the flow, conduction along the thermocouple wires, and radiation to the junction surroundings, respectively. These errors are discussed in the following sections.

Error Due to Flow Velocity

The error due to the flow velocity, as follows, is the difference between the total temperature T_{t_2} and the adiabatic wall temperature T_{aw}, where T_{aw} is given by the standard definition and laminar flow over the junction is assumed:

$$T_{aw} = T_2 + N_{Pr,p}^{1/2} (T_{t_2} - T_2) \qquad (A3)$$

In equation (A3), T_2 is the static temperature inside the shield behind the normal shock. (See fig. 9.) As mentioned in "Probe and Rake Description," the vent-to-inlet area ratios were 50 and 60 percent for probes A and B, respectively; these ratios produce optimum temperature recovery (ref. 10) and correspond to internal Mach numbers of 0.3 and 0.4 for the type A and B probes, respectively. The corresponding errors due to velocity are 6.3° and 4.7°R for cases 1 and 2, respectively. (See table III.)

Conduction Error

For simplicity, conduction errors were computed neglecting radiation. (See fig. 13(a).) First, the convective heat transfer to the thermocouple wires was assumed equal to the conduction along the wires from $n = 0$ to $n = L_1$. The corresponding steady-state, one-dimensional heat balance between the convective heat transfer $\dot{q}_c$ and the conduction heat transfer $\dot{q}_k$ is given as

$$h_p C \left[T_{aw} - T(n)\right] = -k_w A \left(\frac{d^2 T}{dn^2}\right) \qquad (A4)$$

In equation (A4), C is the circumference of a thermocouple wire, A is the cross-sectional area, k_w is the wire conductivity, and h_p is the convection coefficient calculated from equation (A1). Substituting $\theta(n) = T(n) - T_{aw}$ into equation (A4) and solving yields

$$\theta(n) = D_1 \cosh\left[n\left(\frac{4h_p}{d_w k_w}\right)^{1/2}\right] + D_2 \sinh\left[n\left(\frac{4h_p}{d_w k_w}\right)^{1/2}\right] \qquad (A5)$$

Equation (A5) was then solved with the following boundary conditions for $n = 0$:

$$k_w \left(\frac{d\theta}{dn}\right) = h_p \theta \, (n = 0) \qquad (A6)$$

and

$$\theta\,(n=0) = (T_J - T_{aw}) \qquad (A7)$$

In equation (A7), T_J is the temperature of the thermocouple junction. The solution of equation (A5) is

$$T\,(n) - T_{aw} = (T_J - T_{aw}) \left\{ \cosh\left[n\left(\frac{4h_p}{d_w k_w}\right)^{1/2} \right] \right.$$
$$\left. + N_{Bi} \sinh\left[n\left(\frac{4h_p}{d_w k_w}\right)^{1/2} \right] \right\} \qquad (A8)$$

In equation (A8), N_{Bi} is the Biot number and is equal to $(h_p d_w/4k_w)^{1/2}$. The conduction error $T_{aw} - T_J$ could be determined if, for example, the temperature at $n = L_1$ was known. Because space was limited, no additional thermocouples could be located inside the probes; therefore, the heat transfer was also computed along the insulated portion of the thermocouple wire from $n = L_1$ to $n = L_2$, where the assumed wire temperature was 540°R. The corresponding steady-state, one-dimensional heat transfer equation is given as

$$\dot{q} = -k_w A \left(\frac{d\theta}{dn}\right) \qquad (A9)$$

In equation (A9), the heat transfer rate $\dot{q}$ is assumed to be constant along the insulated portion of the thermocouple wire. The solution of equation (A9) is given as

$$\dot{q} = k_w A \frac{T\,(n=L_1) - T\,(n=L_2)}{L_1 - L_2} \qquad (A10)$$

The derivative of equation (A8) was taken at $n = L_1$ to obtain the heat entering the insulated portion of the thermocouple wire. When this expression is combined with equation (A10), $T(n = L_1)$ can be eliminated. The resulting equation for the conduction error is

$$E_k = (T_{aw} - T_J) = \frac{T_{aw} - T\,(n=L_2)}{D_3} \qquad (A11)$$

where $D_3 = D_4 + D_5(L_2 - L_1)$ and

$$D_4 = \cosh\left[L_1 \left(\frac{4h_p}{d_w k_w}\right)^{1/2} \right]$$
$$+ N_{Bi} \sinh\left[L_1 \left(\frac{4h_p}{d_w k_w}\right)^{1/2} \right]$$

$$D_5 = \left(\frac{4h_p}{d_w k_w}\right)^{1/2} \left\{ \sinh\left[L_1 \left(\frac{4h_p}{d_w k_w}\right)^{1/2} \right] \right.$$
$$\left. + N_{Bi} \cosh\left[L_1 \left(\frac{4h_p}{d_w k_w}\right)^{1/2} \right] \right\}$$

The conduction errors $T_{aw} - T_J$ are 2.2°R for case 1 and 85.7°R for case 2, which correspond to 18.0 and 58.9 percent of the total error, respectively. (See table III.) A constant conductivity of 1.20×10^{-3} Btu/sec-in-°R was used in the calculations (ref. 19). This value corresponds to pure platinum at 3200°R and represents the highest conductivity over the temperature range of the analysis (540° to 3200°R); therefore, the result should be a conservative estimate of conduction error.

Radiation Error

For simplicity, radiation errors were computed neglecting conduction, as illustrated in figure 13(b). The steady-state heat balance between the convection to the junction $\dot{q}_{c,J}$ and radiation from the junction to the shield $\dot{q}_{r,J\ \text{to}\ si}$ is given as

$$h_p A_J (T_{aw} - T_J) = A_J \sigma_B F \left(T_J^4 - T_{si}^4 \right) \qquad (A12)$$

In equation (A12), F is the configuration factor for one gray surface that encloses a second surface (ref. 20); thus,

$$F = \frac{1}{\frac{1}{\varepsilon_J} + \frac{A_J}{A_{si}}\left(\frac{1}{\varepsilon_{si}} - 1\right)} \qquad (A13)$$

The steady-state heat balance between the convection to the shield $\dot{q}_{c,si}$, the radiation from the junction to the shield $\dot{q}_{r,J\ \text{to}\ si}$, and the radiation from the shield to the surroundings $\dot{q}_{r,so\ \text{to}\ \infty}$, is given by

$$h_{si} A_{si} (T_{aw} - T_{si}) = A_{so} \sigma_B \varepsilon_{so} \left(T_{so}^4 - T_\infty^4 \right)$$
$$- A_J \sigma_B F \left(T_J^4 - T_{si}^4 \right) \qquad (A14)$$

The convective heat transfer coefficient for the shield near the junction h_{si} was determined from the laminar thermal entry-length solution for flow inside circular tubes (ref. 21). Assuming $T_{si} = T_{so}$, equations (A12) and (A14) were solved iteratively until convergence within 0.5°R. A single value of 0.18 (ref. 19), which corresponds to polished platinum at 3200°R, was used for ε_J, ε_{si}, and ε_{so}. Because the emittance of platinum increases with temperature, a conservative estimate of the radiation errors should result. For cases 1 and 2, the radiation errors $T_{aw} - T_J$ are 3.7° and 55.0°R, which

10

represent 30.3 and 37.8 percent of the total error, respectively.

The total error from this analysis ranged from 12.2° to 145.4°R for the two extremes. These values represent a total error of 0.4 and 6.2 percent, respectively, in the total temperature measurements. Most of the errors that occur at the low probe Reynolds number conditions are estimated to be caused by conduction losses, particularly deep within the boundary layer where the total temperature also is relatively low.

Appendix B

Calculations of Theoretical Probe Thermal Response Time

To simplify the calculations for theoretical thermal response time of the total temperature probes, conduction and radiation losses were neglected. Also, the temperature of the thermocouple junction was assumed to be uniform. The resulting heat transfer equation is

$$h_p A \left[T_t - T_J \left(t \right) \right] = \rho c V \left(\frac{dT_J}{d_t} \right) \qquad \text{(B1)}$$

In equation (B1), A is the projected frontal area of the thermocouple bead, and $\rho, c,$ and V are its density, specific heat, and volume. The values of density and specific heat used in the calculations were 0.775 lbm/in^3 and 0.0314 Btu/lbm°-R; these values correspond to platinum at 540°R (ref. 22). The heat transfer coefficient h_p was determined by calculating $N_{Re,p}$ for a given flow condition and then using equation (A1). The probe Reynolds number can be calculated from the measured total temperature

and pressure behind a normal shock and the probe internal Mach number, computed from the vent-to-inlet area ratio. Substituting $\theta(t) = T_J(t) - T_t$ and $\tau = \rho c V / h_p A$ into equation (B1) and solving yields

$$\theta = C_1 \exp \left(-t/\tau \right) \qquad \text{(B2)}$$

In equation (B2), C_1 is an unknown constant. Application of the initial condition of $\theta(t = 0) = T_J(t = 0) - T_t$ and rearrangment of terms yields

$$\frac{T_J \left(t \right) - T_J \left(t = 0 \right)}{T_t - T_J \left(t = 0 \right)} = 1 - \exp \left(-t/\tau \right) \qquad \text{(B3)}$$

From equation (B3), the thermal response time τ corresponds to the time required for the junction to reach 63.2 percent of the surrounding temperature of the gas after a step change in the gas temperature. For the two extremes in flow conditions, the predicted τ ranged from 0.3 to 1.5 sec. The predicted range for 5τ, which corresponds to the time required for the junction temperature to reach 99.3 percent of the gas temperature, was 1.5 to 7.5 sec. These values are within the model exposure times.

Appendix C

Crocco-Busemann Predictions

To evaluate the total temperature distributions measured in the boundary layer, the linear Crocco-Busemann enthalpy-velocity relationship (ref. 16) was applied. The linear relationship is derived from the energy equation for a two-dimensional, zero pressure gradient boundary layer and from the assumption that $H = H(U)$. This relationship is given as

$$\frac{H_t - H_w}{H_{te} - H_w} = \frac{U}{U_e} \qquad (C1)$$

The linear relationship assumes similarity between the thermal and velocity boundary layers and is valid for boundary layers along isothermal walls with a Prandtl number of unity. However, equation (C1) is considered a reasonable approximation for an air test medium with $N_{Pr} = 0.7$ (ref. 17). For the present

methane-air combustion products test medium, the Prandtl number is nominally 0.76.

To relate total enthalpy to location in the boundary layer, the following power law expression was used:

$$\frac{U}{U_e} = \left(\frac{z}{\delta_U}\right)^{1/N} \qquad (C2)$$

In equation (C2), the exponent N, the velocity boundary-layer thickness δ_U, and the boundary-layer-edge velocity U_e were derived from the pressure and temperature measurements that were obtained in the boundary layer (ref. 11). Combining equations (C1) and (C2) yields

$$H_t = \left(\frac{z}{\delta_U}\right)^{1/N} (H_{te} - H_w) + H_w \qquad (C3)$$

Temperature was inferred from enthalpy with the Mollier charts in reference 18 for methane-air combustion products.

Appendix D

Probe Stress Analysis

The stresses on the shields were analyzed by first assuming that the dominant load was caused by the fluctuating pressures beneath the turbulent boundary layer. Data compiled in reference 23 indicate that the fluctuating pressure beneath a turbulent boundary layer at the wall is 5 percent of the local static pressure at Mach 5. Measurements obtained in the 8'HTT during the present tests (ref. 24) at the same Mach number indicate lower fluctuating pressures, which were 3 percent of the local static pressure. This percentage was used to analyze the stresses on the shields of probes A and B at the highest pressure condition. The loads on the thermocouple wires were determined by treating the wires as circular cylinders that were inclined to the flow at approximately 6°. The flow in the normal direction to the wires was then analyzed. According to the experiments of Gerrard (ref. 25), the dominant fluctuating load for cylinders at subcritical Reynolds numbers is the fluctuating lift. Farell (ref. 26) found that the peak fluctuating lift is of the same order of magnitude as the steady drag. The fluctuating load on the thermocouple wires was estimated at 2.35×10^{-4} lbm with the drag coefficient data compiled by Schlichting (ref. 27). According to the results of Richter and Naudascher (ref. 28), the estimated flow confinement effect of the radiation shield on the steady and fluctuating loads on the thermocouple wires is low. The highest vortex-shedding frequency is estimated at approximately one-half the resonant frequency of the wires.

Both the shield and thermocouple wires were treated as cantilevered beams that were simply supported, and the maximum bending stresses were calculated with the standard equations given in reference 29 as follows:

$$\sigma_{max} = mr/I \qquad (D1)$$

In equation (D1), $I = \pi/64(d_{so}^4 - d_{si}^4)$ for the radiation shield, where I is the cross-sectional moment of inertia. Treating the thermocouple as a single wire for simplicity, $I = \pi/64(d_w^4)$. Also, r is the outside radius of the radiation shield or the radius of the thermocouple wire. The bending moment is given as

$$m = wL^2/2 \qquad (D2)$$

In equation (D2), w is the distributed load per cantilevered length L and is given as $p'A/L$, where p' is the fluctuating pressure and A is the projected area. The maximum bending stress for the shield was calculated from these equations to be 15.7 and 25.5 psi for probes A and B, respectively. The maximum bending stress for the thermocouple wires was calculated to be 0.122 psi.

The factors of safety for the shield and wires were computed by extrapolating the ultimate strength data given in reference 22 for pure platinum at various temperatures to the design temperature of 3300°R. The extrapolated ultimate strength is approximately 1000 psi. For cyclic loading, the fatigue strength is a percentage of the ultimate strength. Although these data are not specifically available for platinum, reference 29 gives a value of 30 percent for nonferrous metals. The resulting factors of safety are 19.1 and 11.8 for the shields of probes A and B, respectively. The factor of safety for the thermocouple wires is even higher at 2450. Because platinum-rhodium alloys have a higher yield strength than pure platinum, at least at room temperature, the factors of safety may actually be higher.

The thermocouple wire should not deflect and contact the radiation shield. The maximum deflection was calculated, assuming that the wire is supported as a cantilevered beam (ref. 29):

$$y_{max} = \frac{wL^4}{8YI} \qquad (D3)$$

In equation (D3), Y is the modulus of elasticity and is given in reference 30 as 15×10^6 psi for platinum–6-percent rhodium at 3200°R. The maximum deflection of the thermocouple wire was calculated to be 1.18×10^{-8} in.

14

References

1. Peecher, D. W.; and Shreeve, R. P.: *Stagnation Temperature Measurement at High Mach Number Using Very Small Probes.* D1-82-0945, Boeing Scientific Research Labs., Jan. 1970. (Available from DTIC as AD 704 962.)

2. Beckwith, Ivan E.; Harvey, William D.; and Clark, Frank L. (appendix A by Ivan E. Beckwith, William D. Harvey, and Christine M. Darden and appendix B by William D. Harvey, Lemuel E. Forrest, and Frank L. Clark): *Comparisons of Turbulent-Boundary-Layer Measurements at Mach Number 19.5 With Theory and an Assessment of Probe Errors.* NASA TN D-6192, 1971.

3. Weinstein, Leonard M.: Hot-Wire Coil Probe for High-Speed Flows. *AIAA J.*, vol. 11, no. 12, Dec. 1973, pp. 1772–1773.

4. Danberg, James E.: *The Equilibrium Temperature Probe, A Device for Measuring Temperatures in Hypersonic Boundary Layers.* NOLTR 61-2, U.S. Navy, Dec. 4, 1961.

5. Winkler, E. M.: *Stagnation Temperature Probes for Use at High Supersonic Speeds and Elevated Temperatures.* NAVORD Rep. 3834, U.S. Navy, Oct. 12, 1954.

6. East, R. A.; and Perry, J. H.: *A Short Time Response Stagnation Temperature Probe.* C.P. No. 909, British Aeronautical Research Council, 1967.

7. Rom, Josef; and Kronzon, Yigal: *Small Shielded Thermocouple Total Temperature Probes.* TAE-79, Israel Inst. of Technology, Dec. 1967. (Available from DTIC as AD 668 466.)

8 Weinstein, Leonard M.: A Shielded Fine-Wire Probe for Rapid Measurement of Total Temperature in High-Speed Flows. *J. Spacecr. & Rockets,* vol. 8, no. 4, Apr. 1971, pp. 425–428.

9. Keener, Earl R.; and Hopkins, Edward J.: *Turbulent Boundary-Layer Velocity Profiles on a Nonadiabatic Flat Plate at Mach Number 6.5.* NASA TN D-6907, 1972.

10. Bartlett, R. P.; Edwards, A. J.; and Hillier, R.: *Development and Calibration of a Total Temperature Probe for the Imperial College Aeronautics Department Gun Tunnel.* IC-AERO-79-02, Imperial College of Science and Technology (London, England), June 1979.

11. Albertson, Cindy W.: Evaluation of Equilibrium Turbulence for a Hypersonic Boundary Layer at Nonadiabatic Wall Conditions. M.S. Thesis, Old Dominion Univ., 1989. (Available as NASA TM-101663, 1989.)

12. Nowak, Robert J.; Albertson, Cindy W.; and Hunt, L. Roane: *Aerothermal Tests of a 12.5° Cone at Mach 6.7 for Various Reynolds Numbers, Angles of Attack, and Nose Shapes.* NASA TP-2345, 1985.

13. Powell, Robert L.; Hall, William J.; Hyink, Clyde H., Jr.; Sparks, Larry L.; Burns, George W.; Scroger, Margaret G.; and Plumb, Harmon H.: *Thermocouple Reference Tables Based on the IPTS-68.* NBS Monogr. 125, U.S. Dep. of Commerce, Mar. 1974.

14. Venkateswaran, S.; Hunt, L. Roane; and Prabhu, Ramadas K.: *Computational Method To Predict Thermodynamic, Transport, and Flow Properties for the Modified Langley 8-Foot High-Temperature Tunnel.* NASA TM-4374, 1992.

15. Moffat, Robert J.: Gas Temperature Measurement. *Temperature Its Measurement and Control in Science and Industry,* Volume 3, Part 2, Reinhold Publ. Corp., c.1962, pp. 553–571.

16. White, Frank M.: *Viscous Fluid Flow.* McGraw-Hill, Inc., c.1974.

17. Fernholz, H. H.; and Finley, P. J.: *A Critical Commentary on Mean Flow Data for Two-Dimensional Compressible Turbulent Boundary Layers.* AGARD-AG-253, May 1980.

18. Leyhe, E. W.; and Howell, R. R.: *Calculation Procedure for Thermodynamic, Transport, and Flow Properties of the Combustion Products of a Hydrocarbon Fuel Mixture Burned in Air With Results for Ethylene-Air and Methane-Air Mixtures.* NASA TN D-914, 1962.

19. Incropera, Frank P.; and DeWitt, David P.: *Fundamentals of Heat and Mass Transfer,* Third ed. John Wiley & Sons, Inc., c.1990.

20. Pitts, Donald R.; and Sissom, Leighton E.: *Schaum's Outline of Theory and Problems of Heat Transfer.* McGraw-Hill, Inc., c.1977.

21. Kays, W. M.; and Crawford, M. E.: *Convective Heat and Mass Transfer,* Second ed. McGraw-Hill, Inc., c.1980.

22. Lyman, Taylor, ed.: *Metals Handbook. Volume I Properties and Selection of Metals,* 8th ed. American Soc. for Metals, c.1961.

23. Bushnell, Dennis M.; Cary, Aubrey M., Jr.; and Harris, Julius E.: *Calculation Methods for Compressible Turbulent Boundary Layers 1976.* NASA SP-422, 1977.

24. Parrott, Tony L.; Jones, Michael G.; and Albertson, Cindy W.: *Fluctuating Pressures Measured Beneath a High-Temperature, Turbulent Boundary Layer on a Flat Plate at a Mach Number of 5.* NASA TP-2947, 1989.

25. Gerrard, J. H.: An Experimental Investigation of the Oscillating Lift and Drag of a Circular Cylinder Shedding Turbulent Vortices. *J. Fluid Mech.,* vol. 11, pt. 2, Sept. 1961, pp. 241–256.

26. Farell, César: *Part I Flow Around Circular Cylinders: Unsteady Loads.* Proj. Rep. No. 188, Univ. of Minnesota, Nov. 1979.

27. Schlichting, Hermann (J. Kestin, transl.): *Boundary-Layer Theory,* Seventh ed. McGraw-Hill Book Co., c.1979.

15

28. Richter, A.; and Naudascher, E.: Fluctuating Forces on a Rigid Circular Cylinder in Confined Flow. *J. Fluid Mech.,* vol. 78, pt. 3, 1976, pp. 561 576.

29. Shigley, Joseph Edward: *Mechanical Engineering Design,* Third ed. McGraw-Hill, Inc., c.1977.

30. Papadakis, E. P.; Fowler, K. A.; Lynnworth, L. C.; Robertson, A.; and Zysk, E. D.: Ultrasonic Measurements of Young's Modulus and Extensional Wave Attenuation in Refractory Metal Wires at Elevated Temperatures With Application to Ultrasonic Thermometry. *J. Appl. Phys.,* vol. 45, no. 6, June 1974, pp. 2409 2420.

Table I. Total Temperature Probe Locations

Designation[a]	z, in., for—	
	Rake A	Rake B
1	[b]0.060	[c]0.035
2	[b].180	[c].100
3	[b].300	[c].165
4	[b].420	[c].230
5	[b].540	[c].295
6	[b].660	[c].360
7	[b].800	[c].425
8	[b]1.000	[c].540
9	[b]1.400	[c].600
10	[b]1.900	[b].800
11	[b]2.500	[b]1.000
12		[b]1.400
13		[b]1.900
14		[c]2.200
15		[b]2.500

[a]See figure 3.
[b]Probe type A. See figure 2(a).
[c]Probe type B. See figure 2(b).

Table II. Combustor and Local Flow Conditions

[Surface pressure and heat transfer measurements were taken during some runs with the rakes removed]

Run	T_{tc}, °R	p_{tc}, psia	α, deg	Rake location x, in.	y, in.	p_{wall}, psia	T_{wall}, °R	M_e	U_e, ft/sec	ρ_e, lbm/ft³	T_e, °R	T_{te}, °R	δ_T, in.	δ_U, in.	$N_{Re,x}$
10	3250	1500	13.05	49.00	0.00	0.92	627	4.99	6210	3.79×10^{-3}	636	3210	0.48	0.47	7.45×10^6
16	3340	1970	12.85	60.00	.00	1.22	624	4.94	6300	4.91	651	3270	.72	.68	11.70
18	3120	2480	12.92	60.00	.00	1.56	604	4.96	6040	6.89	593	3030	.76	.72	16.77
19	3280	1490	12.83	60.00	.00	.91	610	4.98	6080	3.82	623	3110	.69	.66	9.15
22	2590	2320	10.82	60.00	.00	1.04	591	5.05	5390	5.89	462	2530	.72	.55	15.68
24	2610	1740	10.85	60.00	.00	.76	597	5.16	5480	4.33	460	2600	.61	.52	11.81
25	3330	1000	4.97	60.00	.00	.21	573	6.33	6300	1.33	414	3090	.42	.49	4.47
30	3050	1500	12.98	86.12	.00	.93	584	4.95	5920	3.98	612	2990	1.03	.92	13.76
31	3180	2500	13.03	86.12	.00	1.66	632	4.88	6200	6.20	701	3210	1.13	1.03	19.94
32	3230	1500	12.72	86.12	.00	.94	597	4.96	6080	3.93	626	3100	1.00	.97	13.62
33	3140	3280	12.70	86.12	.00	2.12	630	4.92	6080	8.51	652	3140	1.15	1.00	28.56

Table III. Summary of Theoretical Error Calculations

Case 1

$$[N_{Re,p} = 2470; T_t = 3140°R]$$

	Error, °R	Percent of E_t	Percent of T_t
E_U	6.3	51.7	0.2
E_c	2.2	18.0	.1
E_r	3.7	30.3	.1
E_t	12.2	100.0	.4

Case 2

$$[N_{Re,p} = 63; T_t = 2340°R]$$

	Error, °R	Percent of E_t	Percent of T_t
E_U	4.7	3.3	0.2
E_c	85.7	58.9	3.7
E_r	55.0	37.8	2.3
E_t	145.4	100.0	6.2
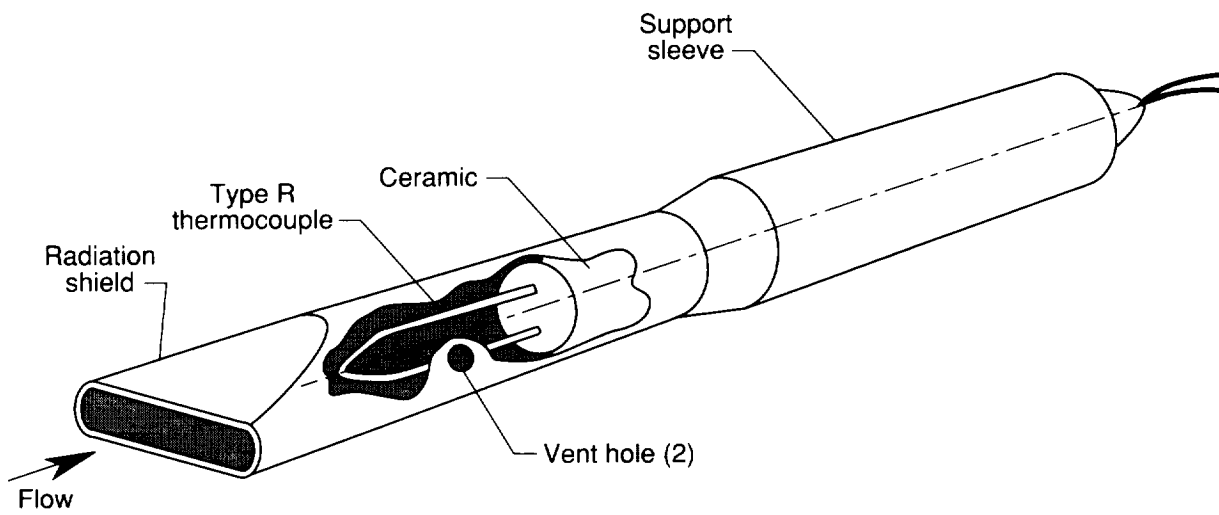
(a) Probe A.
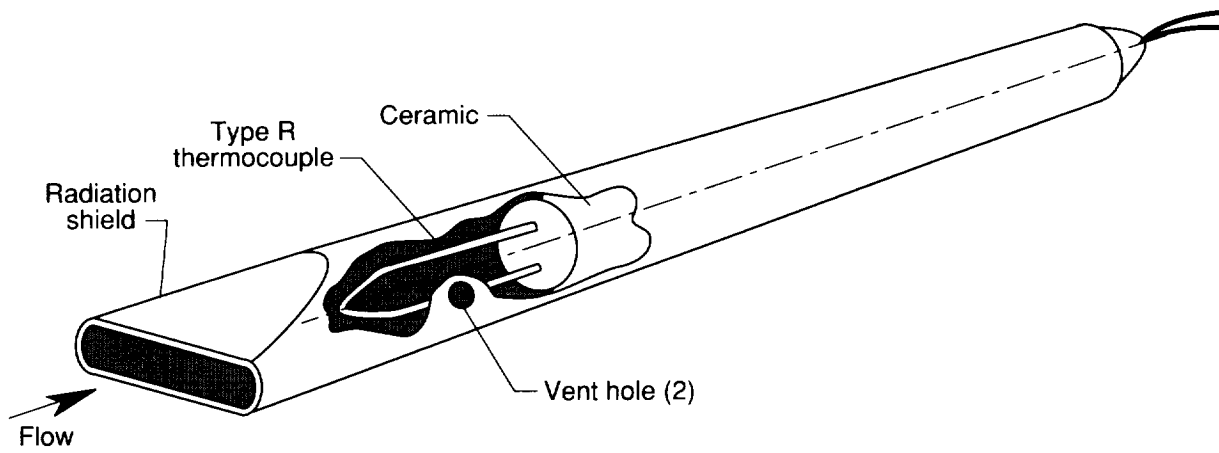
(b) Probe B.

Figure 1. Total temperature probes.

(a) Probe A.

(b) Probe B.
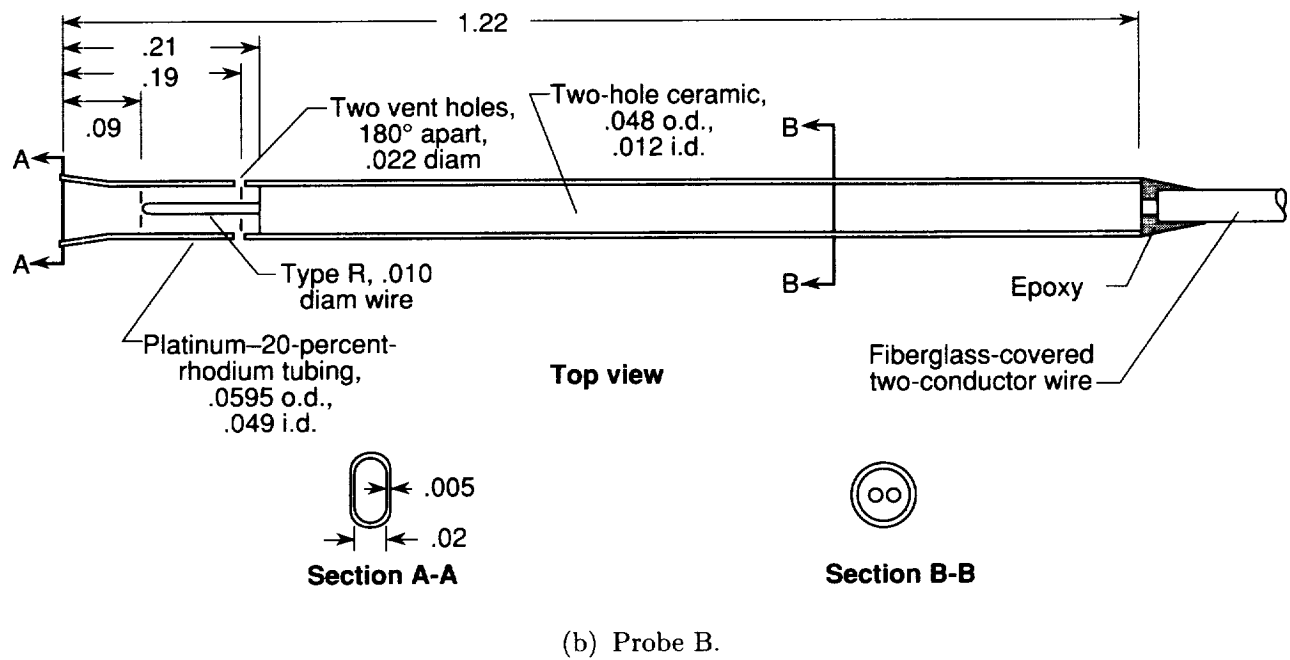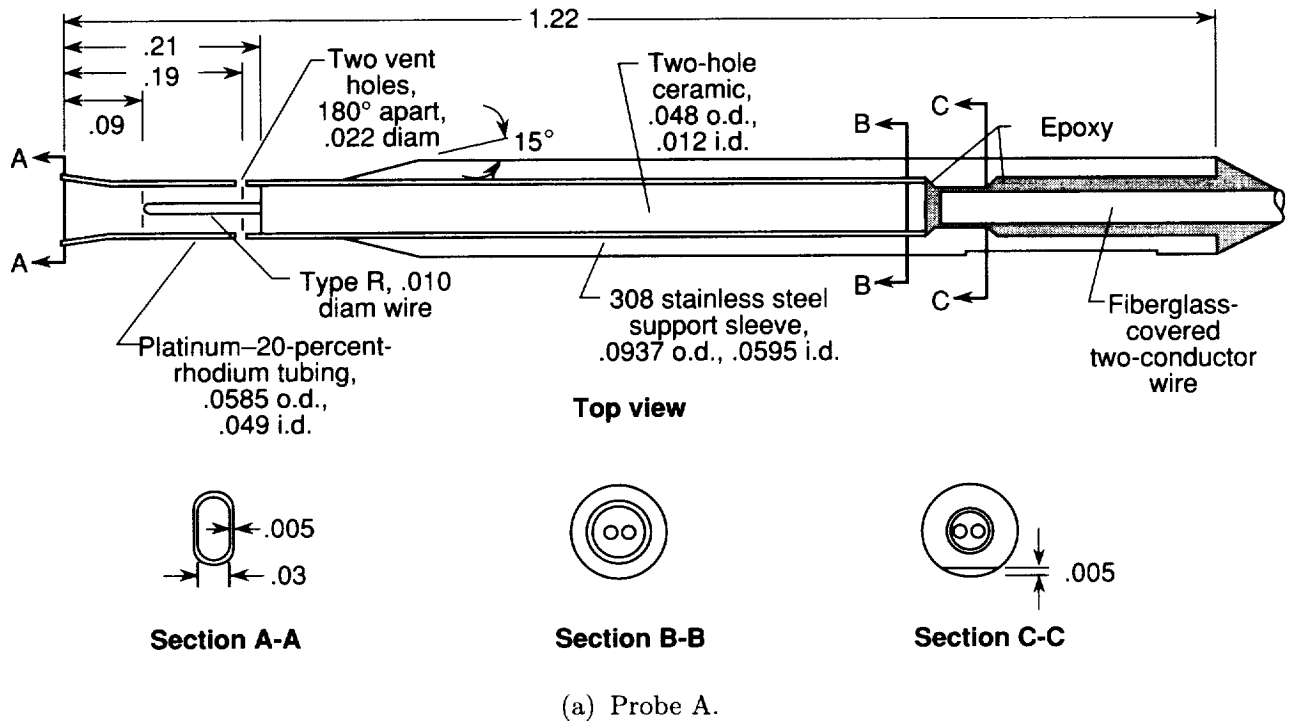
Figure 2. Schematic of total temperature probes. All linear dimensions are in inches.

Top view

Side view
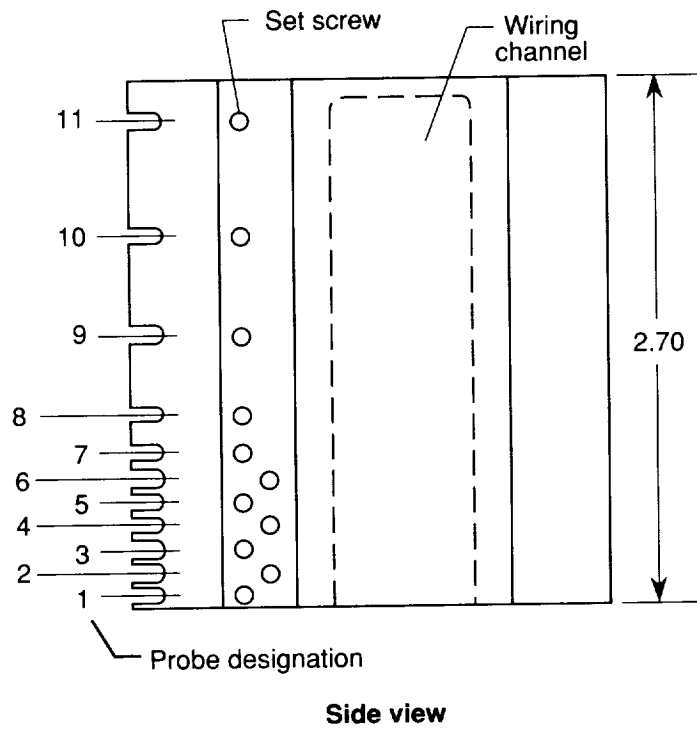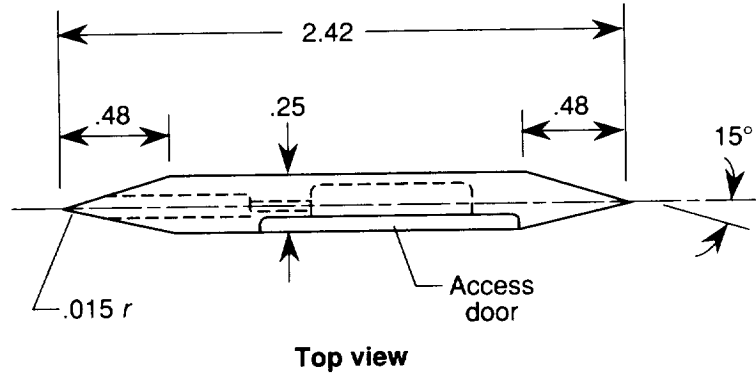
(a) Rake A.

Figure 3. Schematic of total temperature rake without probes. All linear dimensions are in inches.

Top view

Side view
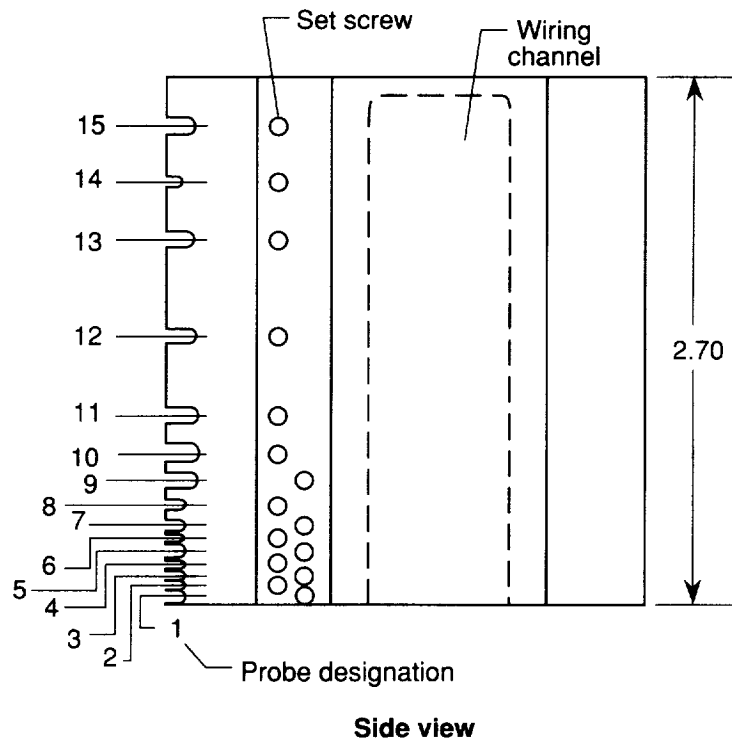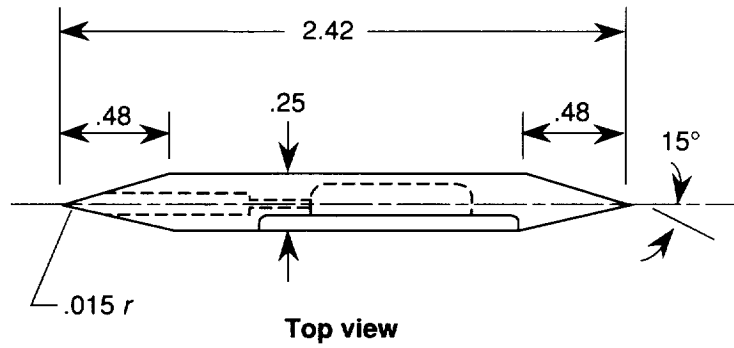
(b) Rake B.

Figure 3. Concluded.
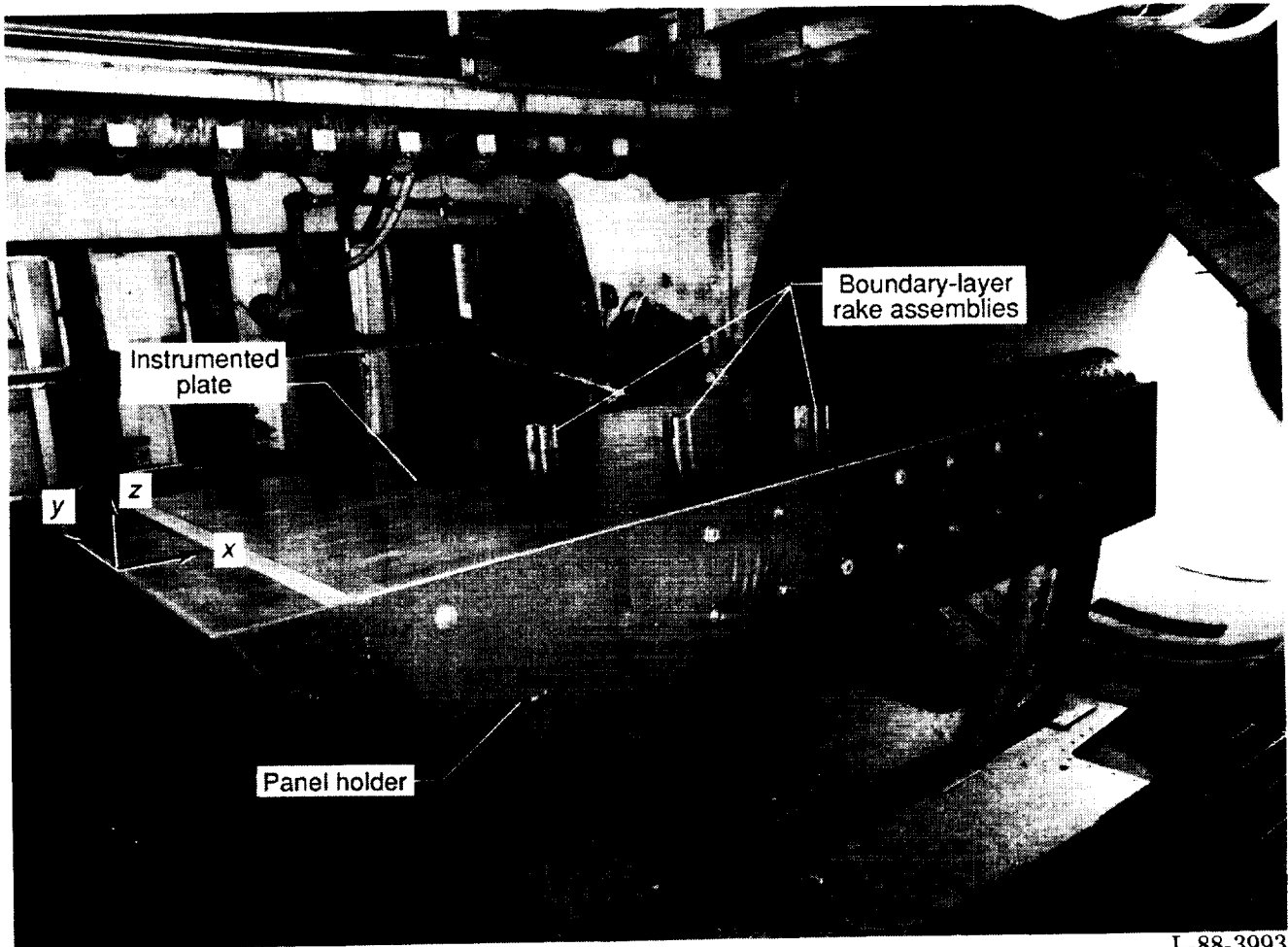
L-88-3993

Figure 4. Panel holder in test chamber of Langley 8-Foot High-Temperature Tunnel.
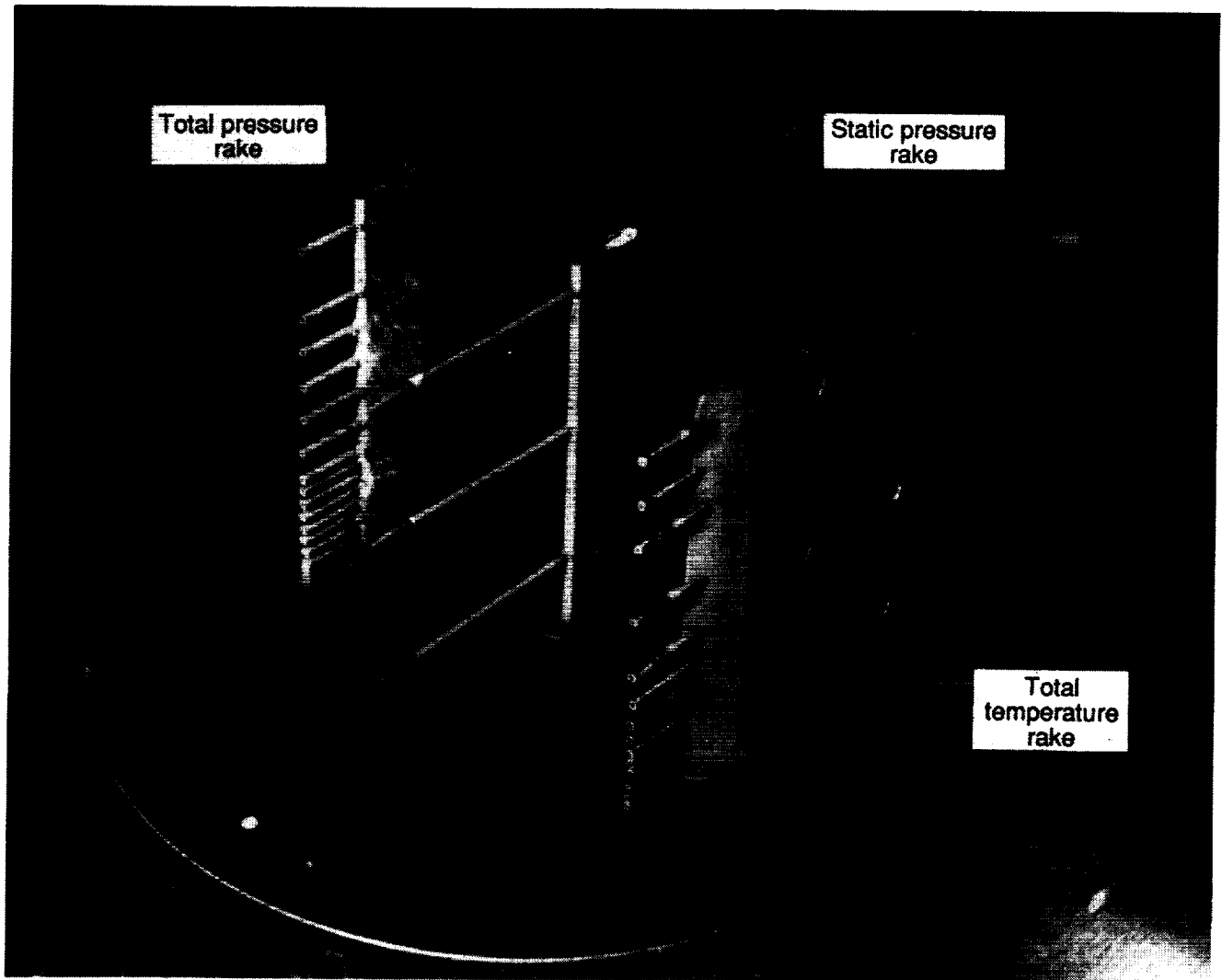
L-88-3994

Figure 5. Boundary-layer rake assembly.
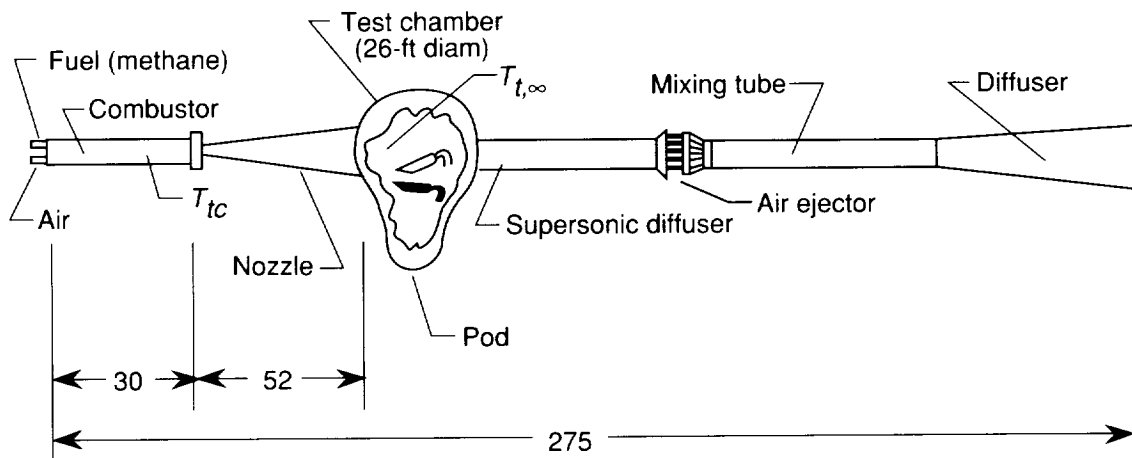
Figure 6. Langley 8-Foot High-Temperature Tunnel. All dimensions are in feet.
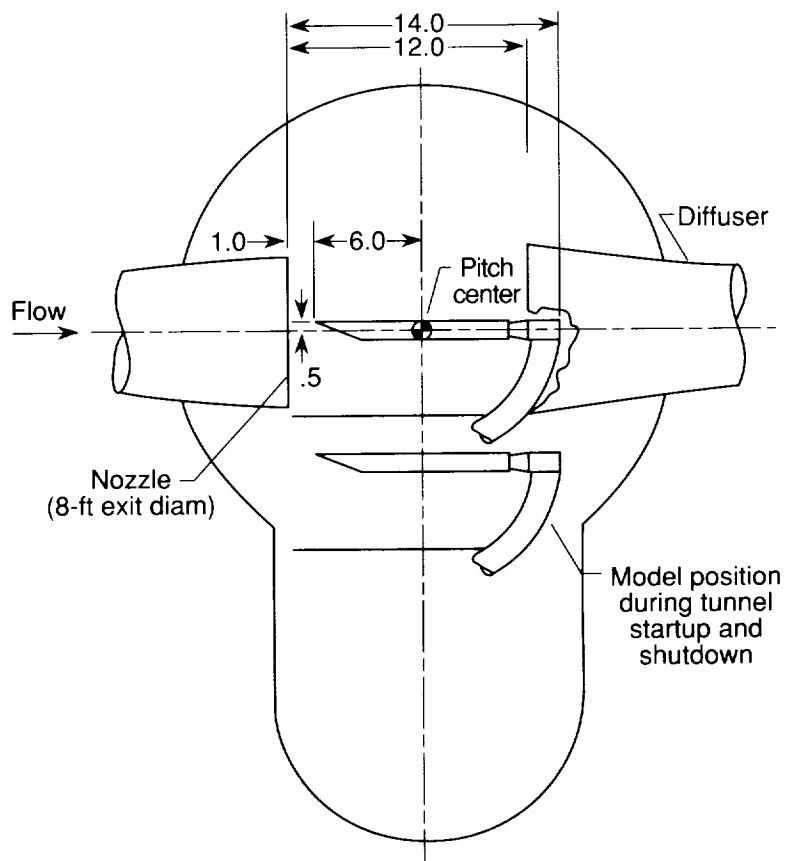
Figure 7. Cross-sectional view of test chamber of Langley 8-Foot High-Temperature Tunnel. All dimensions are in feet.
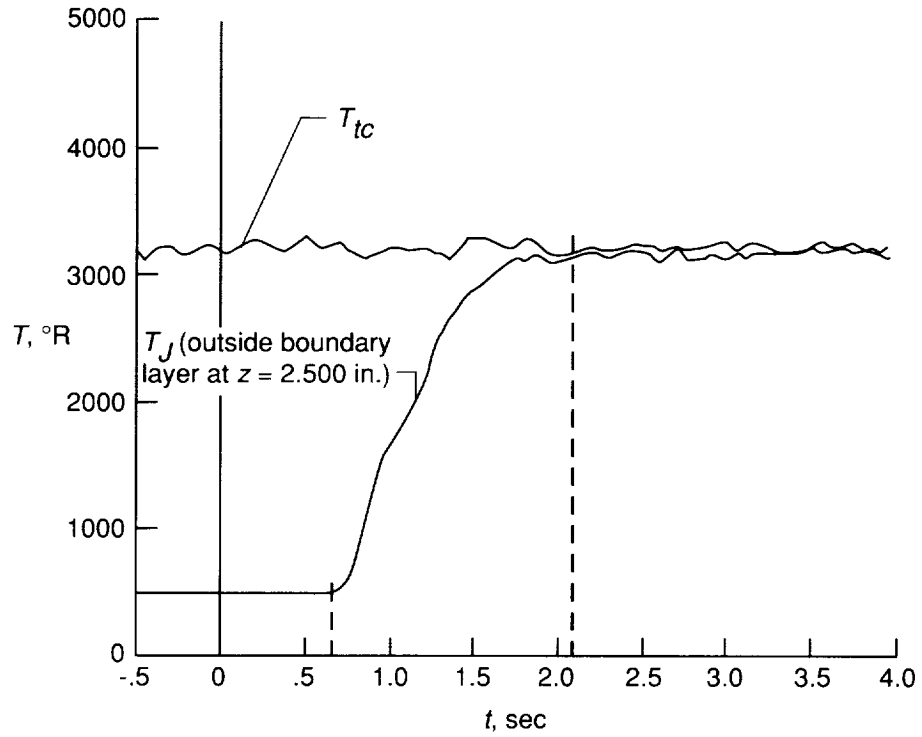
(a) Boundary-layer probe and combustor total temperature histories.
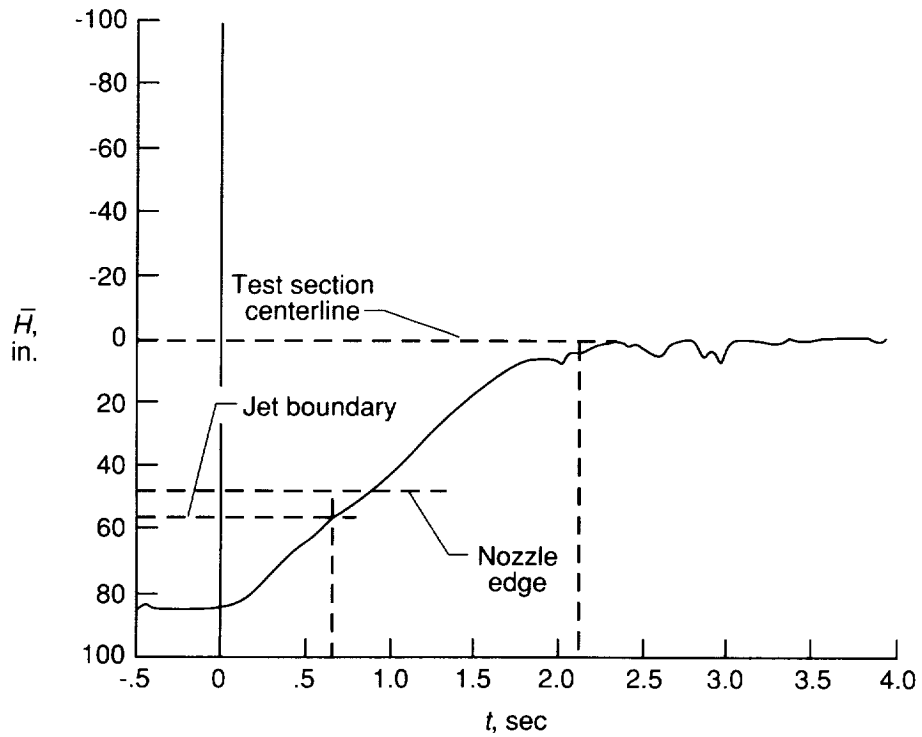
(b) Boundary-layer probe position in test stream.

Figure 8. Typical total temperature and probe position histories. Run 16; $N_{Re,p} = 1016$ at a distance of 72 in. from nozzle exit plane.
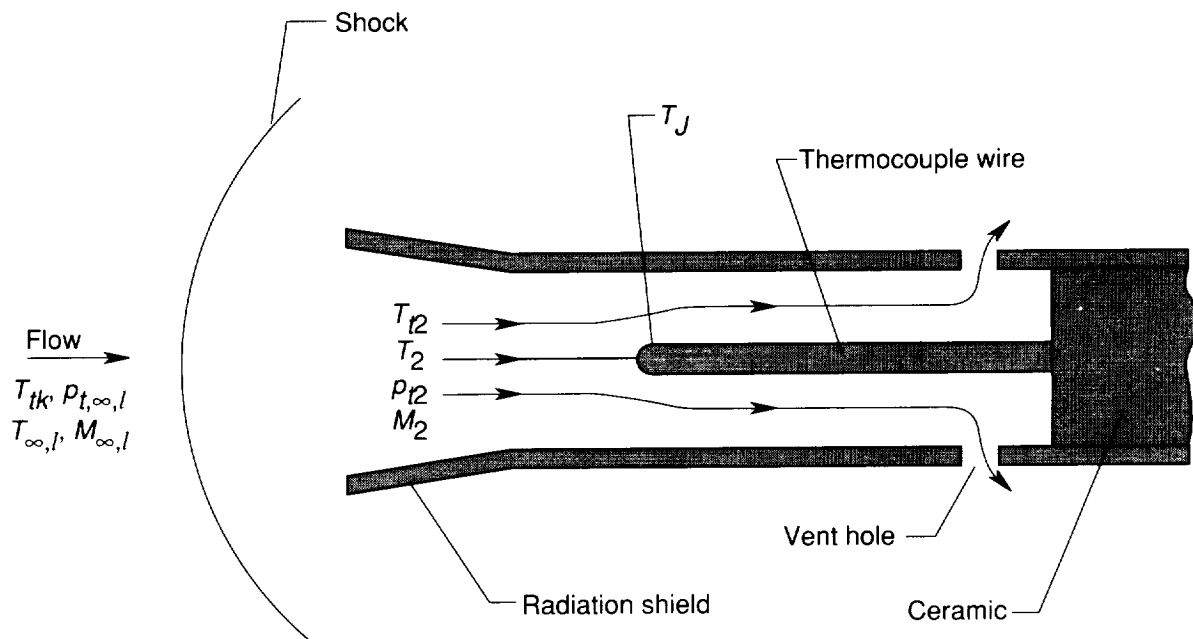
Figure 9. Top view of flow through a total temperature probe.
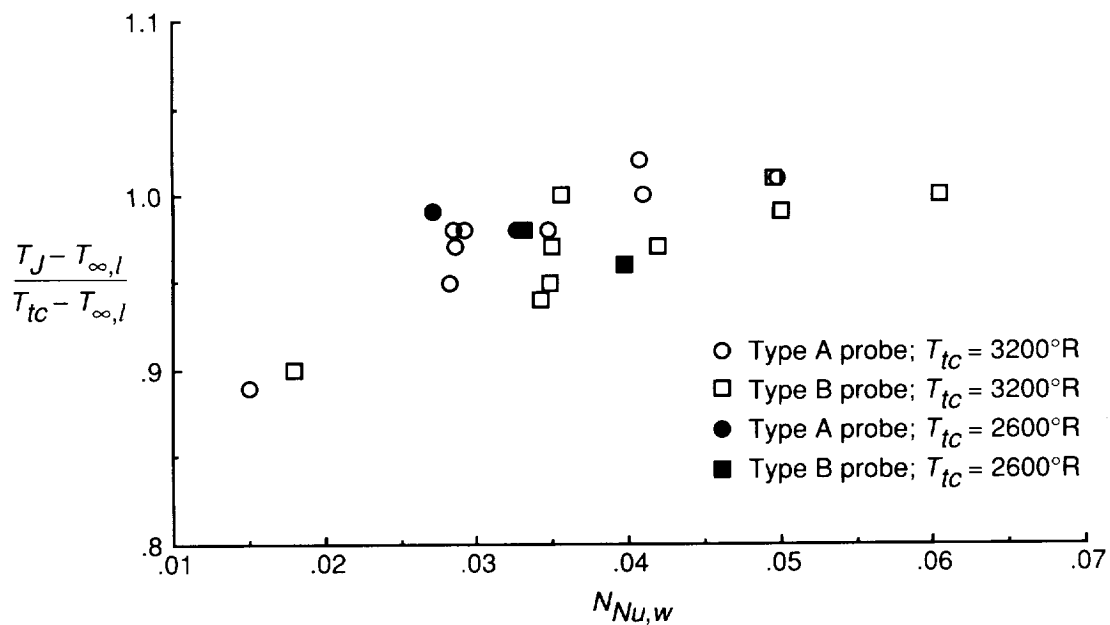
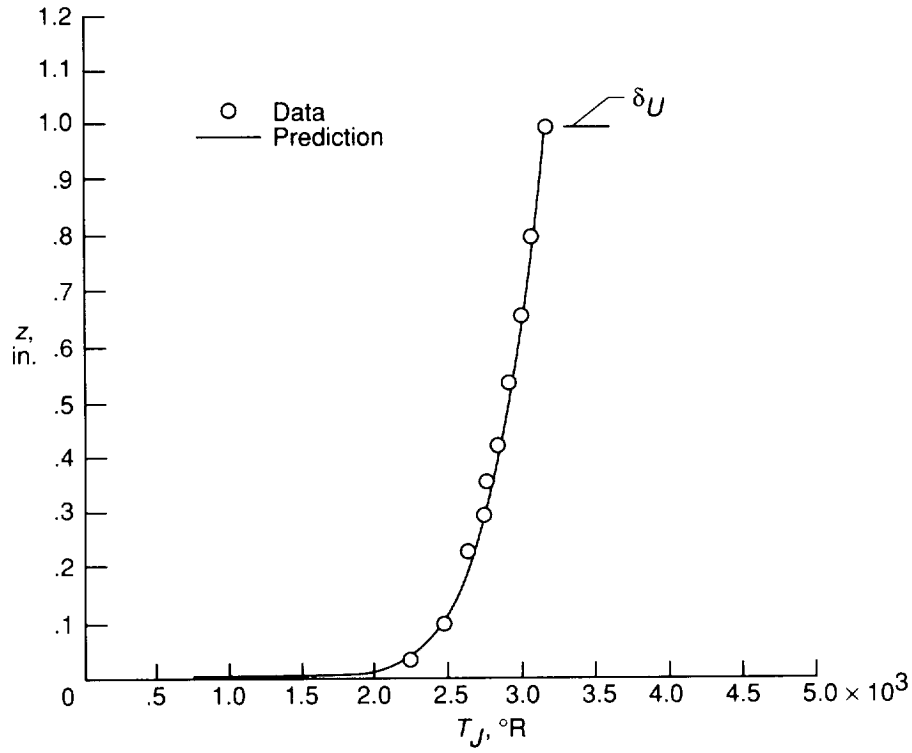Figure 10. Probe recovery factor as a function of Nusselt number based on wire conductivity.
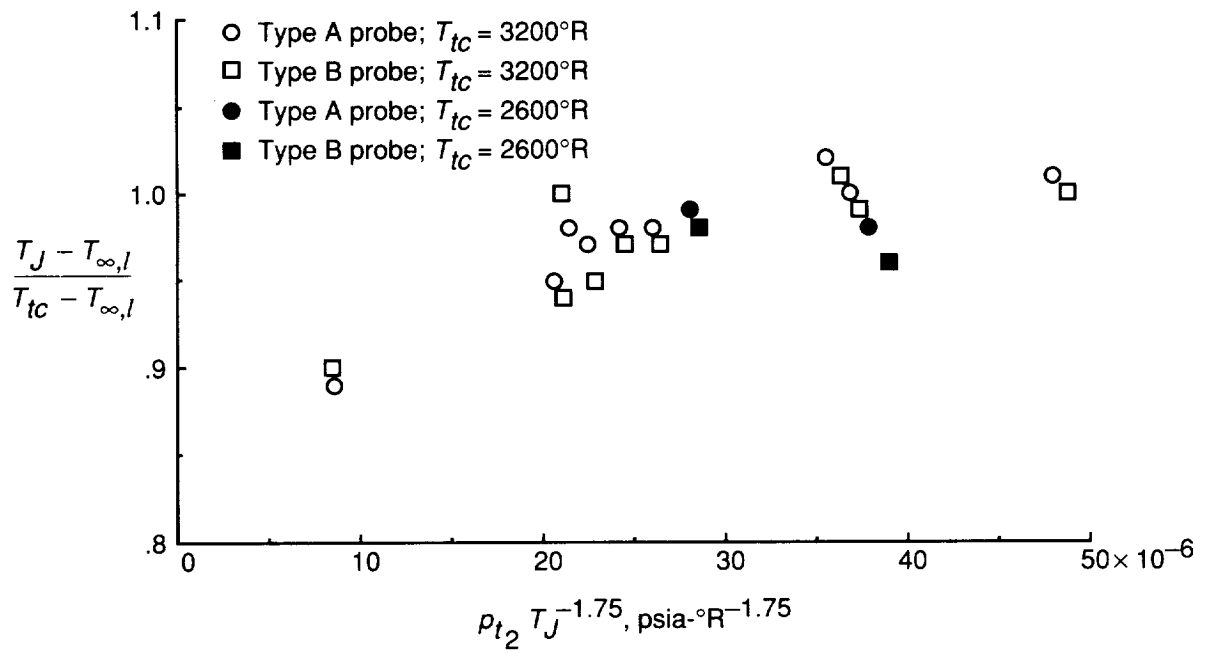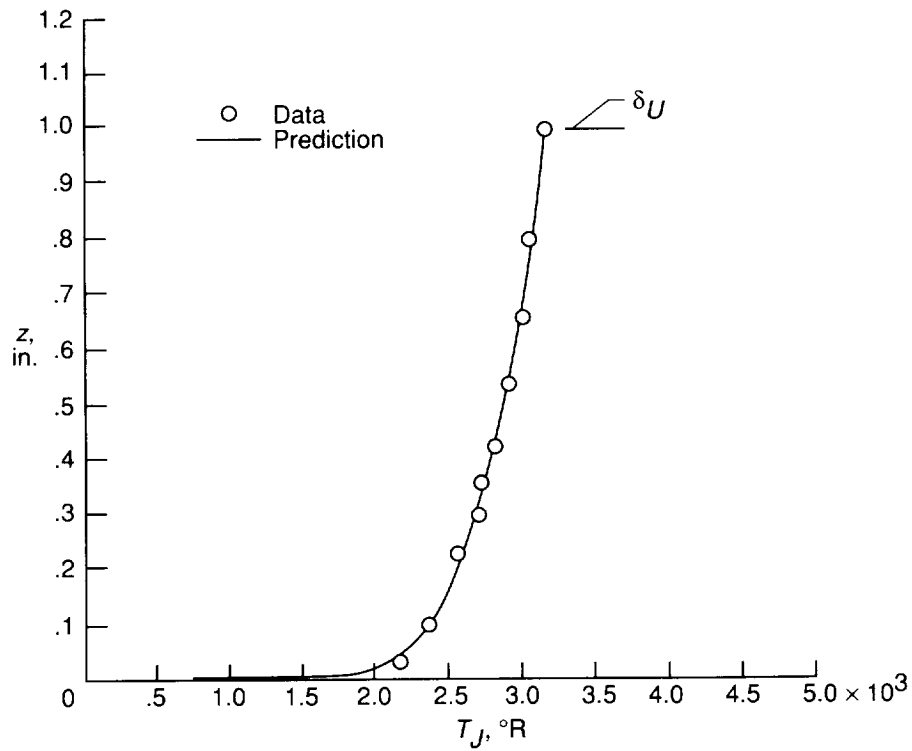
Figure 11. Probe recovery factor as a function of modified Winkler parameter.
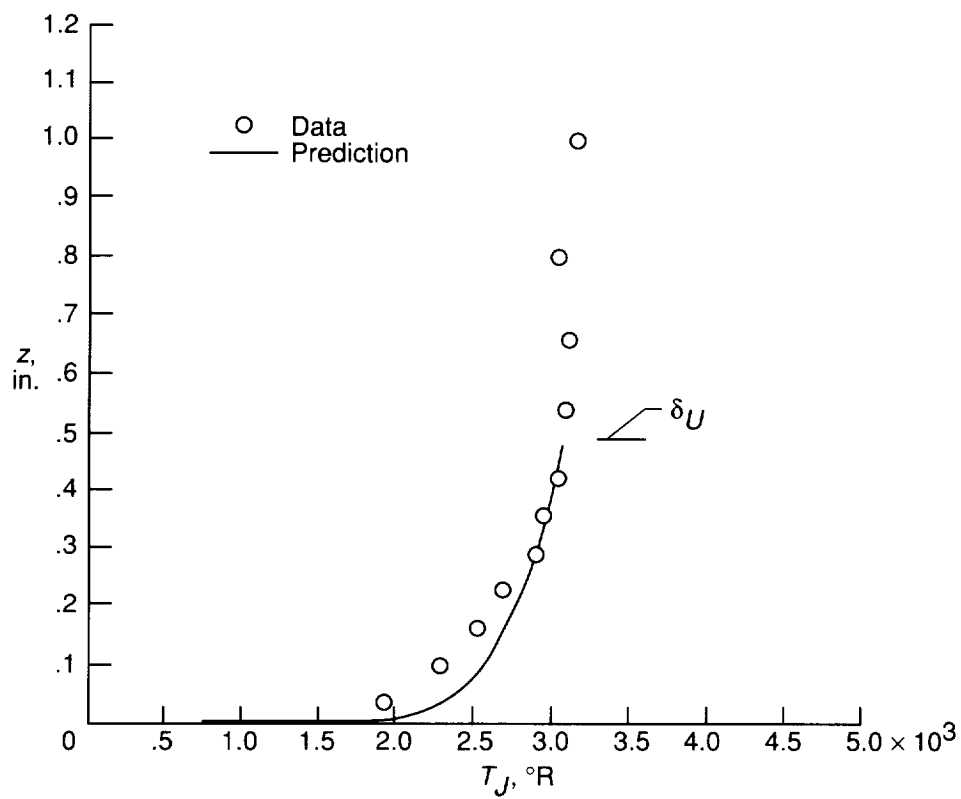
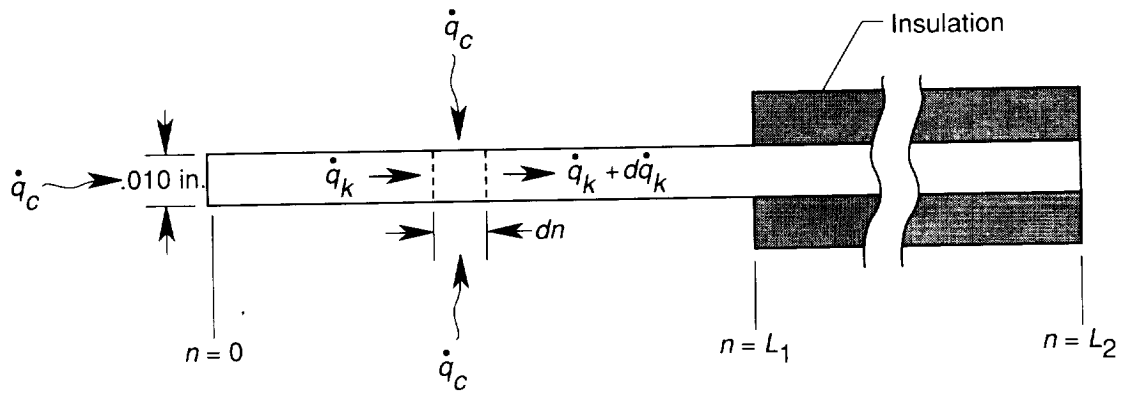(a) $N_{Re,x} = 28.6 \times 10^6$ (run 33).

(b) $N_{Re,x} = 13.6 \times 10^6$ (run 32).

Figure 12. Comparison of total temperature data with Crocco-Busemann predictions.
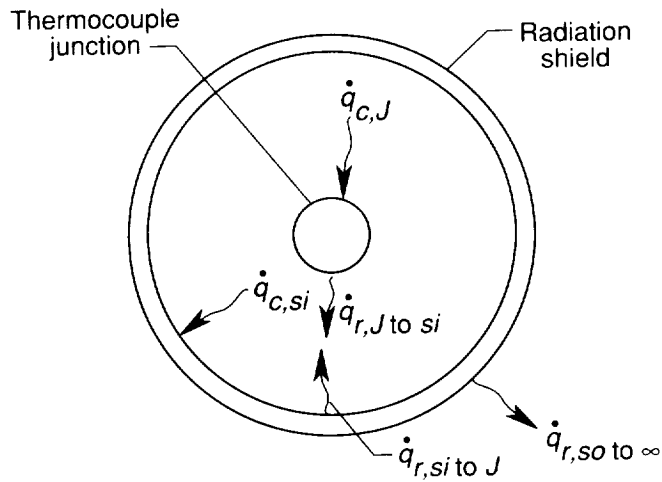
(c) $N_{Re,x} = 4.5 \times 10^6$ (run 25).

Figure 12. Concluded.

(a) Conduction.

(b) Radiation.

Figure 13. Decoupled heat transfer analysis for estimation of probe measurement errors.

REPORT DOCUMENTATION PAGE

Public reporting burden for this collection of information is estimated to average 1 hour per response, including the time for reviewing instructions, searching existing data sources, gathering and maintaining the data needed, and completing and reviewing the collection of information. Send comments regarding this burden estimate or any other aspect of this collection of information, including suggestions for reducing this burden, to Washington Headquarters Services, Directorate for Information Operations and Reports, 1215 Jefferson Davis Highway, Suite 1204, Arlington, VA 22202-4302, and to the Office of Management and Budget, Paperwork Reduction Project (0704-0188), Washington, DC 20503.

1. AGENCY USE ONLY(Leave blank)	2. REPORT DATE	3. REPORT TYPE AND DATES COVERED
	March 1993	Technical Memorandum

4. TITLE AND SUBTITLE

Total Temperature Probes for High-Temperature Hypersonic Boundary-Layer Measurements

5. FUNDING NUMBERS

WU 506-43-21-01

6. AUTHOR(S)

Cindy W. Albertson and Willard A. Bauserman, Jr.

7. PERFORMING ORGANIZATION NAME(S) AND ADDRESS(ES)

NASA Langley Research Center
Hampton, VA 23681-0001

8. PERFORMING ORGANIZATION REPORT NUMBER

L-17124

9. SPONSORING/MONITORING AGENCY NAME(S) AND ADDRESS(ES)

National Aeronautics and Space Administration
Washington, DC 20546-0001

10. SPONSORING/MONITORING AGENCY REPORT NUMBER

NASA TM-4407

11. SUPPLEMENTARY NOTES

12a. DISTRIBUTION/AVAILABILITY STATEMENT

Unclassified Unlimited

Subject Category 35

12b. DISTRIBUTION CODE

13. ABSTRACT *(Maximum 200 words)*

The design and test results of two types of total temperature probes that were used for hypersonic boundary-layer measurements are presented. The intent of each design was to minimize the total error and to maintain minimal size for measurements in boundary layers 1.0 in. thick and less. A single platinum 20-percent-rhodium shield was used in both designs to minimize radiation heat transfer losses during exposure to the high-temperature test stream. The shield of the smaller design was flattened at the flow entrance to an interior height of 0.02 in., compared with 0.03 in. for the larger design. The resulting vent-to-inlet area ratios were 60 and 50 percent. A stainless steel structural support sleeve that was used in the larger design was excluded from the smaller design, which resulted in an outer diameter of 0.059 in., to allow closer placement of the probes to each other and to the wall. These small design changes to improve resolution did not affect probe performance. Tests were conducted at boundary-layer-edge Mach numbers of 5.0 and 6.2. The nominal free-stream total temperatures were 2600° and 3200°R. The probes demonstrated extremely good reliability. The best performance in terms of recovery factor occurred when the wire-based Nusselt number was at least 0.04. Recommendations for future probe designs are included.

14. SUBJECT TERMS

Total temperature probe; High-temperature measurement; Hypersonic boundary layer

15. NUMBER OF PAGES

32

16. PRICE CODE

A03

17. SECURITY CLASSIFICATION OF REPORT	18. SECURITY CLASSIFICATION OF THIS PAGE	19. SECURITY CLASSIFICATION OF ABSTRACT	20. LIMITATION OF ABSTRACT
Unclassified	Unclassified		